

WASP-31b: a low-density planet transiting a late-F-type star \star , $\star\star$

D. R. Anderson¹, A. Collier Cameron², C. Hellier¹, M. Lendl³, T. A. Lister⁴, P. F. L. Maxted¹, D. Queloz³, B. Smalley¹, A. M. S. Smith¹, A. H. M. J. Trias³, R. G. West⁵, D. J. A. Brown², M. Gillon⁶, F. Pepe³, D. Pollacco⁷, D. Ségransan³, R. A. Street⁴, and S. Udry³

¹ Astrophysics Group, Keele University, Staffordshire ST5 5BG, UK

e-mail: dra@astro.keele.ac.uk

² SUPA, School of Physics and Astronomy, University of St. Andrews, North Haugh, Fife KY16 9SS, UK

³ Observatoire de Genève, Université de Genève, 51 Chemin des Maillettes, 1290 Sauverny, Switzerland

⁴ Las Cumbres Observatory, 6740 Cortona Dr. Suite 102, Santa Barbara, CA 93117, USA

⁵ Department of Physics and Astronomy, University of Leicester, Leicester LE1 7RH, UK

⁶ Institut d'Astrophysique et de Géophysique, Université de Liège, Allée du 6 Août, 17, Bat. B5C, Liège 1, Belgium

⁷ Astrophysics Research Centre, School of Mathematics & Physics, Queen's University, University Road, Belfast BT7 1NN, UK

Received February 9, 2009; accepted March 10, 2009

ABSTRACT

We report the discovery of the low-density, transiting giant planet WASP-31b. The planet is 0.47 Jupiter masses and 1.56 Jupiter radii. It is in a 3.4-day orbit around a $\lesssim 1$ -Gyr-old, late-F-type, $V = 11.7$ star, which is a member of a common proper motion pair. In terms of its low density, WASP-31b is second only to WASP-17b, which is a more highly irradiated planet of similar mass.

Key words. binaries: eclipsing – planetary systems – stars: individual: WASP-31

1. Introduction

To date, 107 transiting extrasolar planets have been discovered¹, the majority of which are gas giants in short orbits. The radii of a subset of these exoplanets are larger than predicted by standard models of irradiated gas giants (e.g., Burrows et al. 2007; Fortney et al. 2007), including TrES-4b (Mandushev et al. 2007; Sozzetti et al. 2009), WASP-12b (Hebb et al. 2009), and WASP-17b (Anderson et al. 2010a,c). A number of mechanisms have been proposed as potential solutions to the radius anomaly (see Fortney et al. (2009) for a review), each of which involves either injecting heat into the planet from an external source or slowing heat loss from the planet.

One such mechanism is the dissipation of energy within a planet as heat during the tidal circularisation of an eccentric orbit (Bodenheimer et al. 2001; Gu et al. 2003; Jackson et al. 2008; Ibgui & Burrows 2009). Though these studies found that tidal heating would be sufficient to explain the large radii of even the most bloated exoplanets (although we would have to be observing some systems at very special times), they all truncated the tidal evolution equations to second order in eccentricity. Leconte et al. (2010) recently showed that, other than for near-circular orbits, one must solve the complete tidal equations. Neglecting to do so results in an underestimate of the energy dissipation rate and an overestimate of the timescale over which en-

ergy is dissipated. The consequence is that tidal dissipation can account for the radii of moderately bloated planets, but not the most bloated ones.

Burrows et al. (2007) suggested that enhanced opacities would retard the loss of internal heat and thus slow contraction. These enhanced opacities were implemented by the use of supersolar metallicities, a simplistic approach which neglects the increase in molecular weight that would partially or completely counter the effect on the planet radius (Guillot 2008). Also, strongly irradiated planetary atmospheres are radiative down to deep levels, so heavy elements are likely to settle out. However, atmospheric dynamics may keep the atmosphere well mixed (Showman et al. 2008; Spiegel et al. 2009).

The bloated planets are all very strongly irradiated by their host stars, and a small fraction of stellar insolation energy would be sufficient to account for the observed degrees of bloating. Guillot & Showman (2002) suggested that the kinetic energy of strong winds, induced in the atmosphere by the large day-night temperature contrasts that result from tidal locking, may be transported downward and deposited as thermal energy in the deep interior. However, a mechanism to convert the kinetic energy into thermal energy would still be required. Li & Goodman (2010) and Youdin & Mitchell (2010) found that turbulence is efficient at dissipating kinetic energy. Magnetic drag on weakly ionized winds (Perna et al. 2010) and Ohmic heating (Batygin & Stevenson 2010) are alternative mechanisms. The non-bloated planets too are highly irradiated. Hence, either such a mechanism would either have to act more efficiently on the bloated planets, or some other property must counteract its effect. One such possibility is the presence of a massive core. Indeed, Guillot et al. (2006) and Burrows et al. (2007) found a correlation between the core masses required to reproduce the

^{*} Based in part on observations made with the HARPS spectrograph on the 3.6-m ESO telescope (proposal 085.C-0393) and with the CORALIE spectrograph and the Euler camera on the 1.2-m Euler Swiss telescope, both at the ESO La Silla Observatory, Chile.

^{**} The photometric time-series and radial velocity data used in this work are only available in electronic form at the CDS via anonymous ftp to cdsarc.u-strasbg.fr (130.79.128.5) or via <http://cdsweb.u-strasbg.fr/cgi-bin/qcat?J/A+A/>

¹ 2010 Nov 25, <http://exoplanet.eu>

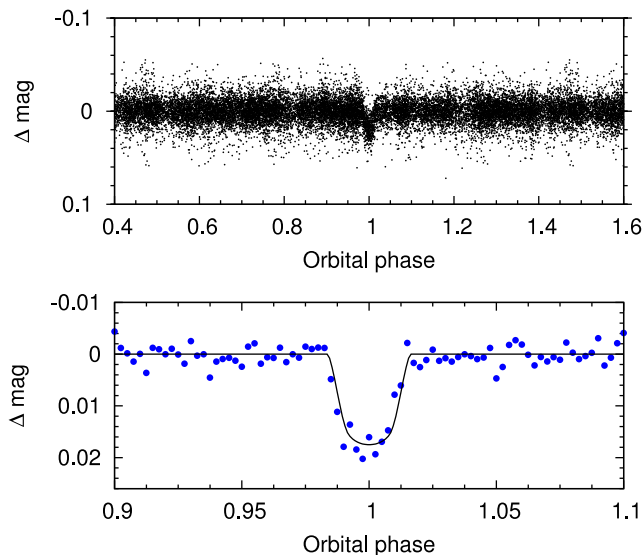


Fig. 1. WASP-South discovery light curve. *Upper panel:* Photometry folded on the orbital period of $P = 3.4$ d. Points with error above three times the median error (0.012 mag) were clipped for display purposes. *Lower panel:* Photometry folded on the orbital period and binned in phase ($\Delta\phi = 0.025$), with the transit model generated from the parameters of Table 2 superimposed.

observed radii of known exoplanets and the metallicities of their host stars.

In this paper, we present the discovery of the bloated, transiting, giant planet WASP-31b. Compared to the ensemble of known short-period planets, WASP-31b is moderately irradiated by its low-metallicity host star.

2. Observations

WASP-31 is a $V = 11.7$, F7–8 star located in the constellation Crater. WASP-31 has been observed by WASP-South (Pollacco et al. 2006) during the first five months of each year since the start of full-scale operations (2006 May 4), and four of these five seasons of data were available at the time of writing. A transit search (Collier Cameron et al. 2006) of the resulting 19 815 usable photometric measurements (Figure 1) found a strong, 3.4-d periodicity.

Using the CORALIE spectrograph mounted on the 1.2-m Euler-Swiss telescope (Baranne et al. 1996; Queloz et al. 2000b), we obtained 34 spectra of WASP-31 during 2009 and a further 13 spectra during 2010. In April 2010, we obtained an additional 10 spectra with the HARPS spectrograph mounted on the 3.6-m ESO telescope. Radial velocity (RV) measurements were computed by weighted cross-correlation (Baranne et al. 1996; Pepe et al. 2005) with a numerical G2-spectral template. RV variations were detected with the same period found from the WASP photometry and with a semi-amplitude of 58 m s^{-1} , consistent with a planetary-mass companion. The RV measurements are plotted in Figure 2.

To test the hypothesis that the RV variations are due to spectral line distortions caused by a blended eclipsing binary, a line-bisector analysis (Queloz et al. 2001) of the CORALIE and HARPS cross-correlation functions was performed. The lack of correlation between bisector span and RV (Figure 2, lower panel), especially for the high-precision HARPS measurements, supports the identification of the transiting body as a planet.

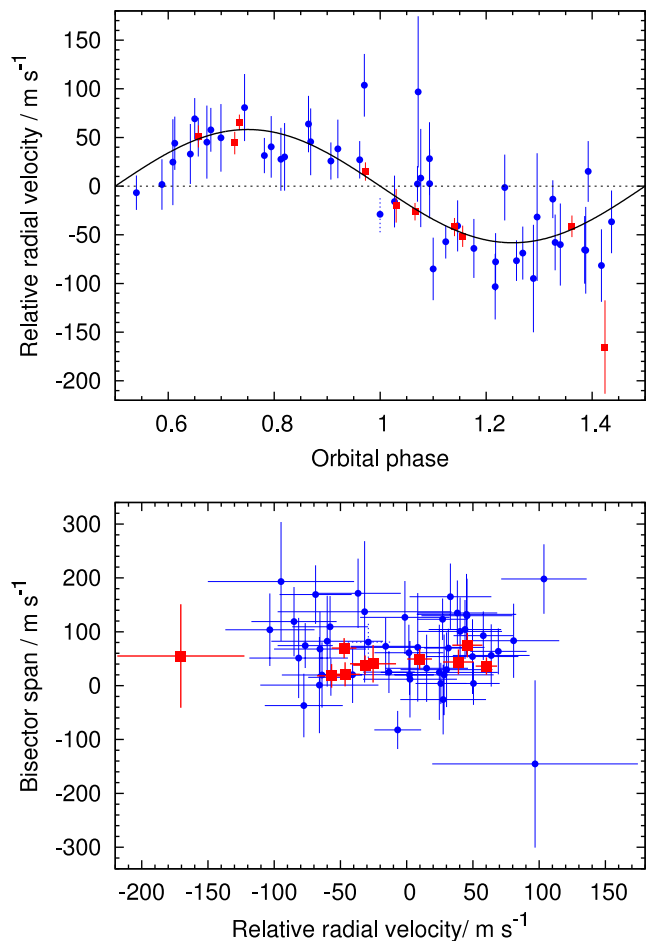


Fig. 2. *Upper panel:* Spectroscopic orbit of WASP-30, as illustrated by CORALIE (blue circles) and HARPS (red squares) radial velocities. The best-fitting Keplerian model, generated from the parameters of Table 2, is overplotted as a solid line. An RV taken at BJD = 2 455 168.8468, depicted in the plot with dotted error bars, fell during transit. As we did not treat the Rossiter-McLaughlin effect (e.g., Queloz et al. 2000a), we excluded this measurement from our combined analysis. *Lower panel:* A lack of correlation between bisector spans and radial velocities rules out a blended eclipsing binary or starspots as the cause of the photometric and spectroscopic variations. We adopted uncertainties on the bisector spans twice the size of those on the radial velocities. For both plots, the centre-of-mass velocity, $\gamma = -125 \text{ m s}^{-1}$, was subtracted from the radial velocities and the Keplerian model.

To refine the system parameters, we obtained high signal-to-noise transit photometry. Photometric follow-up observations of WASP-31 were obtained with the LCOGT² 2.0-m Faulkes Telescope North (FTN) on Mt. Haleakala, Maui on the night of 2010 Feb 26. The fs03 Spectral Instruments camera was used with a 2×2 binning mode giving a field of view of $10' \times 10'$ and a pixel scale of 0.303 arcsec/pixel. The data were taken through a Pan-STARRS-z filter and the telescope was defocussed to prevent saturation and to allow 60-sec exposure times to be used.

The data were pre-processed using the WASP Pipeline (Pollacco et al. 2006) to perform masterbias and flat construction, debiasing and flatfielding. Due to the very low dark current of the fs03 Fairchild CCD ($< 0.0001 \text{ e}^-/\text{pix}/\text{sec}$), dark sub-

² <http://lcogt.net>

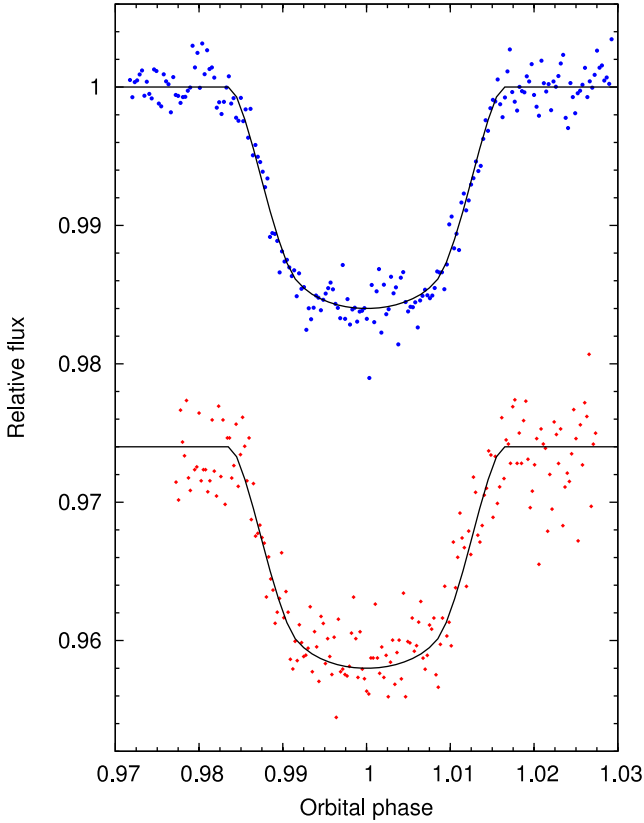


Fig. 3. High signal-to-noise transit light curves. The upper observations (blue circles) were obtained by FTN, using a Pan-STARRS z filter, on 2010 Feb 26. The lower observations (red diamonds), offset in relative flux by 0.026 for display, were obtained by Euler, using a Gunn r filter, on 2010 Apr 15. The best-fitting transit models generated from the parameters of Table 2 are overlotted.

traction was not performed. Aperture photometry was performed using DAOPHOT within the IRAF environment using an aperture with a radius of 11 pixels. Differential photometry was then performed relative to 20 comparison stars that were within the FTN field of view (Figure 3).

On 2010 April 15 we obtained 4.1 hours of photometry in the Gunn r filter with the Euler camera on the Euler-Swiss telescope, covering a complete transit together with 40 and 55 minutes of observations before and after the transit, respectively. The conditions were variable, with seeing ranging from 0.6 arcsec to 1.7 arcsec while an airmass range of 1.15 to 1.34 was covered. Euler now employs absolute tracking to keep the stars on the same pixels during a whole transit. By identifying point sources in each image and matching them with a catalogue, the image centre is calculated. Drifts from the nominal position are then corrected by adjusting the telescope pointing between exposures.

After bias-subtracting and flat-fielding the images, we performed aperture photometry. The flux was extracted for all stars in the field and the final light curve (Figure 3) was obtained by differential photometry of the target and a reference source obtained by combining the 4 brightest reference stars. The average accuracy obtained was 2.7 mmag, which was limited by the number of available reference stars.

Table 1. Stellar parameters from the spectroscopic analysis

Parameter	Value
$T_{*,\text{eff}}$	6300 ± 100 K
$\log g_*$	4.4 ± 0.1 (cgs)
ξ_t	1.4 ± 0.1 km s $^{-1}$
$v \sin i$	7.6 ± 0.4 km s $^{-1}$
[Fe/H]	-0.20 ± 0.09
[Na/H]	-0.24 ± 0.04
[Mg/H]	-0.11 ± 0.06
[Si/H]	-0.13 ± 0.07
[Ca/H]	-0.03 ± 0.08
[Sc/H]	-0.07 ± 0.06
[Ti/H]	-0.10 ± 0.09
[V/H]	-0.16 ± 0.09
[Cr/H]	-0.20 ± 0.08
[Mn/H]	-0.45 ± 0.11
[Ni/H]	-0.25 ± 0.08
$\log A(\text{Li})[\text{LTE}]$	2.82 ± 0.08
$\log A(\text{Li})[\text{NLTE}]$	2.75 ± 0.08
M_*	$1.15 \pm 0.08 M_\odot$
R_*	$1.12 \pm 0.15 M_\odot$
R.A. (J2000) = $11^{\text{h}}17^{\text{m}}45.35^{\text{s}}$	
Dec. (J2000) = $-19^\circ03'17.3''$	
USNO-B1.0 0709-0239208	
2MASS 11174536-1903171	

Note: NLTE Lithium value using correction of Carlsson et al. (1994). Mass and Radius estimate using the Torres et al. (2010) calibration.

3. Stellar parameters

The individual HARPS spectra of WASP-31 were co-added to produce a single spectrum with an average S/N of around 100:1. The analysis was performed using the methods given in Gillon et al. (2009). The H_α line was used to determine the effective temperature ($T_{*,\text{eff}}$), while the Na I D and Mg I b lines were used as surface gravity ($\log g_*$) diagnostics. The parameters obtained from the analysis are listed in Table 1. The elemental abundances were determined from equivalent width measurements of several clean and unblended lines. A value for microturbulence (ξ_t) was determined from Fe I using the method of Magain (1984). The quoted error estimates include that given by the uncertainties in $T_{*,\text{eff}}$, $\log g_*$ and ξ_t , as well as the scatter due to measurement and atomic data uncertainties.

The projected stellar rotation velocity ($v \sin i$) was determined by fitting the profiles of several unblended Fe I lines. We assumed a value for macroturbulence (v_{mac}) of 5.2 ± 0.3 km s $^{-1}$, based on the tabulation by Gray (2008), and we used an instrumental FWHM of 0.06 ± 0.01 Å, determined from the telluric lines around 6300 Å. A best-fitting value of $v \sin i = 7.6 \pm 0.4$ km s $^{-1}$ was obtained. However, recent work by Bruntt et al. (2010) suggests a lower value for macroturbulence of $v_{\text{mac}} = 4.2 \pm 0.3$ km s $^{-1}$ which yields a slightly higher $v \sin i = 8.1 \pm 0.4$ km s $^{-1}$. We therefore adopt the average of these two determinations, $v \sin i = 7.9 \pm 0.6$ km s $^{-1}$. If $v_{\text{mac}} = 0$ km s $^{-1}$, then a value of $v \sin i = 8.7 \pm 0.4$ km s $^{-1}$ is found, which is the upper-limit of the projected rotation velocity.

4. Combined analysis

The WASP, FTN and Euler photometry were combined with the CORALIE and HARPS radial velocities in a simultaneous Markov-chain Monte Carlo (MCMC) analysis (Collier Cameron et al. 2007; Pollacco et al. 2008; Enoch et al. 2010b). The proposal parameters we used are: T_c , P , ΔF , T_{14} , b ,

K_1 , $T_{*,\text{eff}}$, $[\text{Fe}/\text{H}]$, $\sqrt{e} \cos \omega$ and $\sqrt{e} \sin \omega$. Here T_c is the epoch of mid-transit, P is the orbital period, $\Delta F = R_p^2/R_*^2$ is the fractional flux-deficit that would be observed during transit in the absence of limb-darkening, T_{14} is the total transit duration (from first to fourth contact), b is the impact parameter of the planet's path across the stellar disc, K_1 is the stellar reflex velocity semi-amplitude, $T_{*,\text{eff}}$ is the stellar effective temperature, $[\text{Fe}/\text{H}]$ is the stellar metallicity, e is the orbital eccentricity and ω is the argument of periastron.

As Ford (2006) notes, it is convenient to use $e \cos \omega$ and $e \sin \omega$ as MCMC jump parameters, because these two quantities are nearly orthogonal and their joint probability density function is well-behaved when the eccentricity is small and ω is highly uncertain. Ford cautions, however, that the use of $e \cos \omega$ and $e \sin \omega$ as jump parameters implicitly imposes a prior on the eccentricity that increases linearly with e . Instead we use $\sqrt{e} \cos \omega$ and $\sqrt{e} \sin \omega$ as jump parameters, which restores a uniform prior on e .

At each step in the MCMC procedure, each proposal parameter is perturbed from its previous value by a small, random amount. From the proposal parameters, model light and RV curves are generated and χ^2 is calculated from their comparison with the data. A step is accepted if χ^2 (our merit function) is lower than for the previous step; a step with higher χ^2 is accepted with probability $\exp(-\Delta\chi^2/2)$. In this way, the parameter space around the optimum solution is thoroughly explored. The value and uncertainty for each parameter are respectively taken as the median and central 68.3% confidence interval of the parameter's marginalised posterior probability distribution. At each step in the MCMC procedure, we calculate the centre-of-mass velocity, γ , at the fiducial epoch of transit as the mean of the RV residuals about the RV model. We do this separately for the CORALIE and HARPS data, to allow for a systematic instrumental offset, $\Delta\gamma_{\text{HARPS}}$, between the two spectrographs.

From the proposal parameters, we calculate the mass M , radius R , density ρ , and surface gravity $\log g$ of both the star (which we denote with subscript *) and the planet (which we denote with subscript P), as well as the equilibrium temperature of the planet $T_{\text{p,eql}}$ assuming it to be a black-body and that energy is efficiently redistributed from the planet's day-side to its night-side. We also calculate the transit ingress and egress durations, T_{12} and T_{34} , and the orbital semi-major axis a .

With eccentricity floating, we find $e = 0.027^{+0.034}_{-0.020}$. Applying the 'F-test' of Lucy & Sweeney (1971), we find a 66% probability that an eccentricity of or above the fitted value could have arisen by chance if the underlying orbit is in fact circular. As such, we impose a circular orbit, but we note that doing so has no significant effect as the fitted eccentricity was so small.

The median parameter values and their $1-\sigma$ uncertainties from our MCMC analysis are presented in the middle column of Table 2. The corresponding best-fitting transit light curves are shown in Figure 1 and Figure 3, and the best-fitting RV curve is shown in Figure 2.

Without exquisite photometry, our implementation of MCMC tends to bias the impact parameter, and thus R_* and R_p , to higher values. This is because, with low signal-to-noise photometry, the transit ingress and egress durations are uncertain, and symmetric uncertainties in those translate into asymmetric uncertainties in b and thus in R_* . The effect on the stellar and planetary radii is larger for high-impact-parameter planets such as WASP-31b. Therefore we explored an MCMC with a main-sequence (MS) prior imposed (Collier Cameron et al. 2007). This employs a Bayesian penalty to ensure that, in accepted steps, the values of stellar radius are consistent with the values of stellar mass for

Table 2. System parameters from the combined analysis

Parameter (Unit)	no MS prior (adopted solution)	with MS prior
P (d)	3.405909 ± 0.000005	3.405909 ± 0.000005
T_c (HJD-2450000)	5189.2828 ± 0.0003	5189.2828 ± 0.0003
T_{14} (d)	0.1107 ± 0.0014	0.1093 ± 0.0012
$T_{12} = T_{34}$ (d)	0.0276 ± 0.0020	0.0257 ± 0.0016
$\Delta F = R_p^2/R_*^2$	0.01622 ± 0.00032	0.01596 ± 0.00029
b	0.769 ± 0.016	0.752 ± 0.016
i ($^\circ$)	84.54 ± 0.27	84.81 ± 0.23
K_1 (m s^{-1})	58.2 ± 3.5	58.0 ± 3.5
a (AU)	0.04657 ± 0.00034	0.04662 ± 0.00035
e	0 (adopted)	0 (adopted)
γ_{CORALIE} (m s^{-1})	-124.924 ± 0.036	-124.922 ± 0.036
$\Delta\gamma_{\text{HARPS}}$ (m s^{-1})	-5.268 ± 0.096	-5.264 ± 0.096
M_* (M_\odot)	1.161 ± 0.026	1.165 ± 0.026
R_* (R_\odot)	1.241 ± 0.039	1.206 ± 0.035
ρ_* (ρ_\odot)	0.608 ± 0.052	0.664 ± 0.050
$\log g_*$ (cgs)	4.316 ± 0.024	4.341 ± 0.021
$T_{*,\text{eff}}$ (K)	6203 ± 98	6339 ± 99
$[\text{Fe}/\text{H}]$	-0.19 ± 0.09	-0.18 ± 0.09
M_p (M_{Jup})	0.478 ± 0.030	0.477 ± 0.030
R_p (R_{Jup})	1.537 ± 0.060	1.482 ± 0.053
ρ_p (ρ_{Jup})	0.132 ± 0.017	0.146 ± 0.017
$\log g_p$ (cgs)	2.665 ± 0.042	2.696 ± 0.038
$T_{\text{p,eql}}$ (K)	1568 ± 33	1555 ± 33

Table 3. Proper motions of WASP-31 and its visual companion

Star	Catalogue	μ_{RA} (mas)	μ_{Dec} (mas)
WASP-31	UCAC3	-28.2 ± 1.3	-0.4 ± 1.6
WASP-31	PPXML	-25.0 ± 2.3	-0.1 ± 2.4
Companion	UCAC3	-33.1 ± 3.1	$+1.0 \pm 3.8$
Companion	PPXML	-28.5 ± 4.2	$+1.6 \pm 4.2$

a main-sequence star. The difference between the solutions with and without MS priors is small (Table 2), indicating that the transit light curves are of a quality such that the ingress and egress durations are measured sufficiently well. As such, we adopt the solution without the MS prior, which has more conservative error bars.

5. System age

WASP-31 is a visual double with a $V \sim 15.8$ star (2MASS 11174477-1903521) approximately $35''$ away³. The 2MASS colours of the companion suggest that it is a mid-to-late K-type star. The proper motions for the two stars listed in the PPMXL (Roeser et al. 2010) and UCAC3 (Zacharias et al. 2010) catalogues suggest that this is a common proper motion pair (Table 3).

Using 2MASS photometry we constructed a colour-magnitude diagram (Figure 4). A distance modulus of 8.0 ± 0.2 (400 ± 40 pc) is required to place the companion on the main-sequence, and this puts WASP-31 very close to the zero-age

³ The companion is blended with WASP-31 in the WASP images. Though it is 40 times fainter than WASP-31 and it is resolved in the Euler and FTN images, we did correct the WASP photometry for the contamination prior to producing the MCMC solution presented. We checked the effect of the contamination by producing another MCMC solution using the non-corrected WASP photometry. The best-fitting parameter values were the same to within a tenth of an error bar.

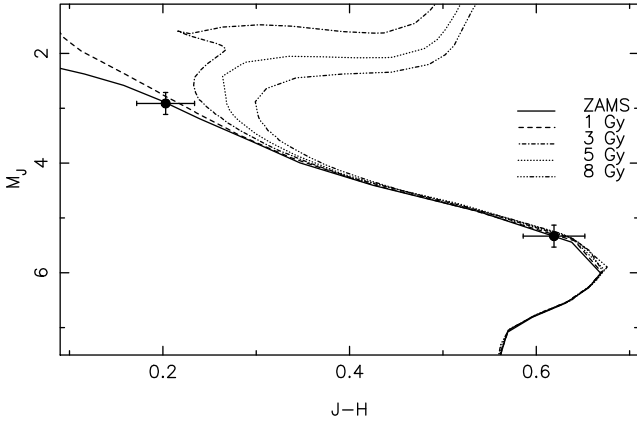


Fig. 4. Colour-magnitude diagram for WASP-31 and its companion. Various isochrones from Marigo et al. (2008) are given, with ages indicated in the figure.

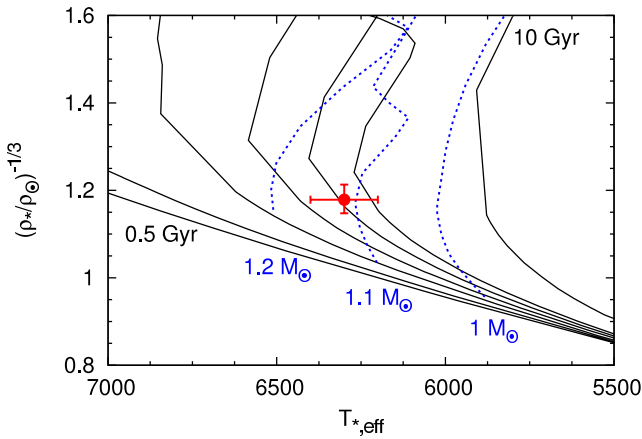


Fig. 5. Modified H-R diagram. The evolutionary mass tracks ($Z = 0.017 \approx [\text{Fe}/\text{H}] = -0.05$; $Y = 0.30$) and isochrones ($Z = 0.012 \approx [\text{Fe}/\text{H}] = -0.20$) for the ages 0.5, 1, 2, 3, 4, 5 and 10 Gyr are from Marigo et al. (2008).

main sequence and 1-Gyr age lines. At a distance of 400 pc, the two stars would be separated by at least 14 000 AU (0.2 light-year).

Assuming aligned stellar-spin and planetary-orbit axes, the measured $\nu \sin i$ of WASP-31 and its derived stellar radius indicate a rotational period of $P_{\text{rot}} = 8.0 \pm 0.7$ d. Combining this with the $B - V$ colour of an F6 star from Gray (2008), we used the relationship of Barnes (2007) to estimate a gyrochronological age of $1.5^{+1.3}_{-0.6}$ Gyr. We found no evidence for rotational modulation in the WASP light curves.

The lithium abundance ($A_{\text{Li}} = 2.75 \pm 0.10$) found in WASP-31 implies an age (Sestito & Randich 2005) between that of open clusters such as M34 (250 Myr; $A_{\text{Li}} = 2.92 \pm 0.13$) and NGC 752 (2 Gyr; $A_{\text{Li}} = 2.65 \pm 0.13$). However, lithium is a poor indicator of age for a star as hot as WASP-31, and the measured abundance is consistent at the $1\text{-}\sigma$ level with that of the upper envelope of the 5-Gyr M67 ($A_{\text{Li}} = 2.55 \pm 0.18$).

We interpolated the stellar evolution tracks of Marigo et al. (2008) using ρ_* from the MCMC analysis and using $T_{*,\text{eff}}$ and $[\text{Fe}/\text{H}]$ from the spectral analysis (Figure 5). This suggests an age of 4 ± 1 Gyr and a mass of $1.12 \pm 0.05 M_{\odot}$ for WASP-31.

6. Discussion

With a mass of $0.48 M_{\text{Jup}}$ and a radius of $1.54 R_{\text{Jup}}$, WASP-31b has a density 13 per cent that of Jupiter and is $\sim 0.3 R_{\text{Jup}}$ larger than predicted by standard models of irradiated gas giants (Fortney et al. 2007). Only WASP-17b (Anderson et al. 2010a), which has a similar mass ($0.49 M_{\text{Jup}}$), is known to have a lower density ($0.06 \rho_{\text{Jup}}$, Anderson et al. 2010c).

With an increasingly large sample of well-characterised planets, we can begin to make statistical inferences as to the physical reasons behind their diverse natures. Enoch et al. (2010a) showed the radii of 16 of the 18 known low-mass ($0.1\text{--}0.6 M_{\text{Jup}}$) planets strongly correlate with equilibrium temperature and host-star metallicity. The calibration of Enoch et al. (2010a) predicts a radius of $1.39 R_{\text{Jup}}$ for WASP-31b. In a similar study, but using a different metallicity dependence and treating the 74 known Jupiter-mass ($0.2\text{--}2.5 M_{\text{Jup}}$) planets, Anderson et al. (2010b) also found a strong correlation between planetary radius and equilibrium temperature and host-star metallicity. The calibration of Anderson et al. (2010b) predicts a radius of $1.23 R_{\text{Jup}}$ for WASP-31b. In each case, the predicted radius of WASP-31b is smaller than the measured radius ($1.54 \pm 0.06 R_{\text{Jup}}$).

WASP-31 has a similarly low metallicity to WASP-17 ($[\text{Fe}/\text{H}] = -0.19 \pm 0.09$; Triaud et al. 2010), thus both could reasonably be expected to have small cores (Guillot et al. 2006; Burrows et al. 2007). However, this would only somewhat explain why the two planets are so large. Both planets are highly irradiated, with WASP-17b being more irradiated than WASP-31b as, despite being in a slightly wider orbit ($a = 0.052$ AU), its host star is larger ($R_* = 1.58 R_{\odot}$) and hotter ($T_{*,\text{eff}} = 6650$ K; Anderson et al. 2010c). This results in an equilibrium temperature for WASP-17b hotter by 200 K than for WASP-31b and, from this, we could expect WASP-17b to be larger than WASP-31b. Both planets, though, are larger than predicted by standard models of irradiated giant planets (e.g. Fortney et al. 2007), and by the empirical relations of Enoch et al. (2010a) and Anderson et al. (2010b). Hence, it seems likely that some additional physics is at play.

The RV data place a stringent upper limit on WASP-31b's orbital eccentricity ($e < 0.13$; 3σ). It is therefore unlikely that tidal heating resulting from the circularisation of an eccentric orbit (e.g. Bodenheimer et al. 2001) was responsible for significantly inflating the planet. However, we could happen to be viewing the system soon after circularisation occurred and prior to the planet significantly contracting. This would have made finding the planet easier due to the greater transit depth.

The metallicity of WASP-31 is at the lower end of what may be expected for a star of its age in the Solar neighbourhood (at a Galactocentric radius of 8.5 kpc; Magrini et al. 2009).

Acknowledgements. WASP-South is hosted by the South African Astronomical Observatory and we are grateful for their ongoing support and assistance. Funding for WASP comes from consortium universities and from the UK's Science and Technology Facilities Council. M. Gillon acknowledges support from the Belgian Science Policy Office in the form of a Return Grant.

References

- Anderson, D. R., Hellier, C., Gillon, M., et al. 2010a, *ApJ*, 709, 159
- Anderson, D. R. et al. 2010b, in preparation
- Anderson, D. R. et al. 2010c, in preparation
- Baranne, A., Queloz, D., Mayor, M., et al. 1996, *A&AS*, 119, 373
- Barnes, S. A. 2007, *ApJ*, 669, 1167
- Batygin, K. & Stevenson, D. J. 2010, *ApJ*, 714, L238
- Bodenheimer, P., Lin, D. N. C., & Mardling, R. A. 2001, *ApJ*, 548, 466
- Bruntt, H., Bedding, T. R., Quirion, P., et al. 2010, *MNRAS*, 405, 1907

- Burrows, A., Hubeny, I., Budaj, J., & Hubbard, W. B. 2007, *ApJ*, 661, 502
- Carlsson, M., Rutten, R. J., Bruls, J. H. M. J., & Shchukina, N. G. 1994, *A&A*, 288, 860
- Collier Cameron, A., Pollacco, D., Street, R. A., et al. 2006, *MNRAS*, 373, 799
- Collier Cameron, A., Wilson, D. M., West, R. G., et al. 2007, *MNRAS*, 380, 1230
- Enoch, B., Cameron, A. C., Anderson, D. R., et al. 2010a, *MNRAS*, 1531
- Enoch, B., Collier Cameron, A., Parley, N. R., & Hebb, L. 2010b, *A&A*, 516, A33+
- Ford, E. B. 2006, *ApJ*, 642, 505
- Fortney, J. J., Baraffe, I., & Militzer, B. 2009, *ArXiv e-prints*
- Fortney, J. J., Marley, M. S., & Barnes, J. W. 2007, *ApJ*, 659, 1661
- Gillon, M., Smalley, B., Hebb, L., et al. 2009, *A&A*, 496, 259
- Gray, D. F. 2008, *The Observation and Analysis of Stellar Photospheres*, ed. Gray, D. F.
- Gu, P., Lin, D. N. C., & Bodenheimer, P. H. 2003, *ApJ*, 588, 509
- Guillot, T. 2008, *Physica Scripta Volume T*, 130, 014023
- Guillot, T., Santos, N. C., Pont, F., et al. 2006, *A&A*, 453, L21
- Guillot, T. & Showman, A. P. 2002, *A&A*, 385, 156
- Hebb, L., Collier-Cameron, A., Loicillet, B., et al. 2009, *ApJ*, 693, 1920
- Ibgui, L. & Burrows, A. 2009, *ApJ*, 700, 1921
- Jackson, B., Greenberg, R., & Barnes, R. 2008, *ApJ*, 681, 1631
- Leconte, J., Chabrier, G., Baraffe, I., & Levrard, B. 2010, *A&A*, 516, A64+
- Li, J. & Goodman, J. 2010, *ArXiv e-prints*
- Lucy, L. B. & Sweeney, M. A. 1971, *AJ*, 76, 544
- Magain, P. 1984, *A&A*, 134, 189
- Magrini, L., Sestito, P., Randich, S., & Galli, D. 2009, *A&A*, 494, 95
- Mandushev, G., O'Donovan, F. T., Charbonneau, D., et al. 2007, *ApJ*, 667, L195
- Marigo, P., Girardi, L., Bressan, A., et al. 2008, *A&A*, 482, 883
- Pepe, F., Mayor, M., Queloz, D., et al. 2005, *The Messenger*, 120, 22
- Perna, R., Menou, K., & Rauscher, E. 2010, *ApJ*, 719, 1421
- Pollacco, D., Skillen, I., Collier Cameron, A., et al. 2008, *MNRAS*, 385, 1576
- Pollacco, D. L., Skillen, I., Cameron, A. C., et al. 2006, *PASP*, 118, 1407
- Queloz, D., Eggenberger, A., Mayor, M., et al. 2000a, *A&A*, 359, L13
- Queloz, D., Henry, G. W., Sivan, J. P., et al. 2001, *A&A*, 379, 279
- Queloz, D., Mayor, M., Weber, L., et al. 2000b, *A&A*, 354, 99
- Roeser, S., Demleitner, M., & Schilbach, E. 2010, *AJ*, 139, 2440
- Sestito, P. & Randich, S. 2005, *A&A*, 442, 615
- Showman, A. P., Menou, K., & Cho, J. 2008, in *Astronomical Society of the Pacific Conference Series*, Vol. 398, *Astronomical Society of the Pacific Conference Series*, ed. D. Fischer, F. A. Rasio, S. E. Thorsett, & A. Wolszczan, 419–+
- Sozzetti, A., Torres, G., Charbonneau, D., et al. 2009, *ApJ*, 691, 1145
- Spiegel, D. S., Silverio, K., & Burrows, A. 2009, *ApJ*, 699, 1487
- Torres, G., Andersen, J., & Giménez, A. 2010, *A&A Rev.*, 18, 67
- TriAUD, A. H. M. J., Collier Cameron, A., Queloz, D., et al. 2010, *ArXiv e-prints*
- Youdin, A. N. & Mitchell, J. L. 2010, *ApJ*, 721, 1113
- Zacharias, N., Finch, C., Girard, T., et al. 2010, *AJ*, 139, 2184